LIMNOLOGY
and
OCEANOGRAPHY

ASLO

Limnol. Oceanogr. 64, 2019, 1135–1149

doi: 10.1002/lno.11103

Intertidal regions changing coastal alkalinity: The Wadden Sea-North Sea tidally coupled bioreactor

Yoana G. Voynova,[1*] **Wilhelm Petersen**,[1] **Martina Gehrung**,[1] **Steffen Aßmann**,[2] **Andrew L. King**[3]

[1]Institute of Coastal Research, Helmholtz-Zentrum Geesthacht, Geesthacht, Germany
[2]Kongsberg Maritime Contros GmbH, Kiel, Germany
[3]Norwegian Institute for Water Research, Oslo, Norway

Abstract

In this study, we successfully implemented a total alkalinity (TA) analyzer in a flow-through setup, in combination with a FerryBox. The high-frequency (10 min) measurements along our ship's route revealed that in coastal systems, where carbon fluxes are dynamic, TA can differ significantly (by up to 100 μmol kg^{-1}) between the nearshore and adjacent coastal regions. Even though this study could not account for the net yearly TA production in the coastal region, it demonstrated that there was a seasonal increase in TA of 100–150 μmol kg^{-1} in coastal waters of the North Sea, equivalent to TA production of 11.7–26.8 mmol m^{-2} d^{-1} during the spring and summer months. This seasonal change could not be accounted for by riverine contributions, but instead was probably related to seasonal organic matter production and processing in coastal and nearshore regions. Bottom sediments and the tidally coupled biogeochemical reactor between coastal (North Sea) and nearshore (Wadden Sea) regions are mediating this TA change, and the ~ 4 months lag between the seasonal increase in alkalinity and the peak organic matter production could be explained by the supply of (labile) organic matter and its temperature-dependent remineralization via both aerobic and anaerobic pathways.

Coastal seas and continental shelves connect the land, ocean, and atmospheric carbon reservoirs, and play a crucial role in the global carbon cycle, supporting at least 10% of the ocean carbon dioxide (CO_2) uptake, 30% of oceanic primary production, and 80% of the organic matter burial (Gattuso et al. 1998; Borges et al. 2006; Bauer et al. 2013; Regnier et al. 2013). However, these regions can be quite variable, and regional characteristics must be considered when estimating carbon budgets (Borges 2005; Duarte et al. 2013). Continental shelves, for example, can be either a source or a sink of carbon to the atmosphere, depending on latitude, with those at mid-latitudes generally considered a sink and those at low latitudes considered a source of CO_2 to the atmosphere (Borges 2005; Cai et al. 2006). At the same time, regional characteristics like bathymetry can separate coastal systems into mixed shallow regions, which act as a CO_2 sources, and deeper stratified regions, which act as CO_2 sinks (Thomas et al. 2004, 2005).

A net internal total alkalinity (TA) generation has the potential to increase the capacity of the coastal ocean buffer and the uptake of atmospheric carbon dioxide (CO_2) (Brasse et al. 1999; Chen 2002; Wallmann et al. 2008; Thomas et al. 2009; Hu and Cai 2011*a*; Krumins et al. 2013; Carstensen et al. 2018). However, estimates of global TA generation from anaerobic processes in continental shelves and oxygen minimum zones are widely variable (Gustafsson et al. 2014), ranging from 4–5 Tmol yr^{-1} (Hu and Cai 2011*a*) to 16–31 Tmol yr^{-1} (Chen 2002; Thomas et al. 2009). Net TA generation depends on the reduction of organic matter by denitrification of allochtonous nitrate (Hu and Cai 2011*b*), generation of iron sulfides by sulfate reduction, with subsequent formation of pyrite (Hu and Cai 2011*a*; Brenner et al. 2016), or dissolution of $CaCO_3$ in marine sediments. Examining the influence of intertidal regions, where these reaction rates are high, and determining their influence on the adjacent coastal regions could provide insights into the seasonal cycle of TA, and help elucidate the potential sources of TA.

Sandy sediments, salt marshes, and intertidal flats are so-called biogeochemical reactors, where organic matter from the adjacent coastal areas and the overlying water column is deposited and subsequently remineralized. The remineralized nutrients are released from pore waters back to the overlying water column and the adjacent coastal areas, providing a tight

*Correspondence: yoana.voynova@hzg.de

Additional Supporting Information may be found in the online version of this article.

coupling between the benthic and pelagic communities via tidal circulation (Postma 1981; Anschutz et al. 2009; Beck and Brumsack 2012; Voynova et al. 2015). This coupling could provide remineralized nutrients and TA to surface waters, therefore continually sustaining primary production when other nutrient sources become scarce (Santos et al. 2014).

Using the Wadden Sea-North Sea region as an example of a nearshore to coastal tidally coupled region, this study examines TA changes over 10 months, with the aim to elucidate sources and sinks within the coastal region. Here, we present the first long-term high-resolution (10 min sampling interval) time series of surface-water TA measured via a state-of-the-art analyzer, the CONTROS HydroFIA TA, combined with a FerryBox aboard a moving platform. This sampling setup enabled seasonal and regional TA observations over a large coastal region (> 300 km), and this study links these observations to potential TA sources or sinks. Specifically, we propose that seasonal changes in TA and organic matter in coastal waters are connected to the processing of imported organic matter and potential TA generation in the adjacent nearshore intertidal regions. This study aims to improve our understanding of the use of state-of-the-art TA analyzers, and of the variability and sources of TA in coastal environments.

Methods

Study site

The Wadden Sea (Fig. 1) is one of the largest sandy barrier island ecosystems in the world (Beck and Brumsack 2012), representing a network of sand and mudflats (< 10 m), which stretches 500 km along the coasts of The Netherlands, Germany, and Denmark (van Beusekom et al. 1999). It is characterized as tidal flat and barrier island depositional system with extensive salt marshes, which has remained fairly undisturbed. An ecological transition between land and ocean, with a wide intertidal zone intersected by deep gullies, the Wadden Sea can function as a gigantic coastal filter, as tides import organic matter from the North Sea (Postma 1981). The imported organic matter is mineralized in the marshes, tidal flats, and shallow areas. The remineralized nutrients fuel high regional primary production, and this bioreactor is constantly renewed via the tidal flow (Marencic 2009; Santos et al. 2014, 2015).

Adjacent to the Wadden Sea is the relatively shallow (10–43 m) German Bight, situated in the south-eastern part of the North Sea (Fig. 1). The distribution of temperature and salinity in the bottom layers of the German Bight is strongly related to topography, and follows the ancient Elbe River Valley (Becker et al. 1999). The German Bight is dominated by a counterclockwise residual circulation pattern, which carries a mixture of Atlantic water and continental runoff from the Elbe, the Rhine, and several other rivers into the German Bight from the west (Hickel et al. 1993; van Beusekom et al. 1999). While the central part of the North Sea is

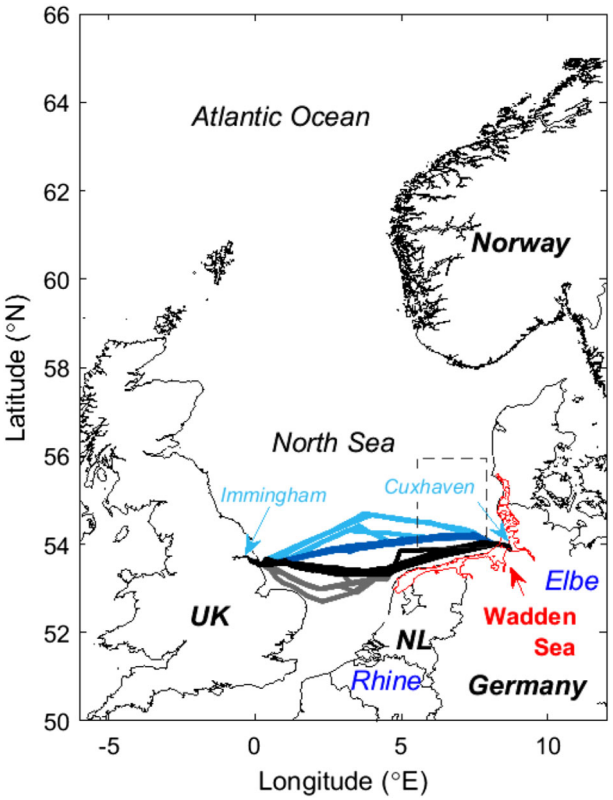

Fig. 1. Map of the North Sea, Wadden Sea (red line), and Hafnia seaways routes between Cuxhaven, DE and Immingham, UK during 2017. The area of the German Bight is roughly outlined with a dashed box. Hafnia Seaways routes in 2017 (January 1 - October 31) are divided in north (light and dark blue) and south (black and gray) transects.

seasonally stratified, the southeast German Bight and the Wadden Sea regions are generally well mixed due to strong tidal currents (Becker et al. 1999).

The North Sea is a large shelf sea that is considered as a major sink for CO_2 (Thomas et al. 2004), and is an excellent site for investigating carbon cycling and sequestration. High-biological productivity, stimulated by large nutrient influxes, and efficient use of nutrients, mediates the carbon dioxide drawdown from the atmosphere to the subsurface layers via the biological and shelf pumps (Thomas et al. 2004). Up to 50% of the carbon exported from the shelf is transported below the permanent thermocline and thus, it is isolated from release to the atmosphere on centennial timescales (Wakelin et al. 2012). The North Atlantic has a large influence on the North Sea circulation and lateral mixing (Otto et al. 1990; Huthnance 1997; Holt and Proctor 2008), and the residence time in the North Sea is relatively short, approximately 1 yr (Otto et al. 1990). Therefore, material produced in the surface, and transported to the bottom stratified layer, could be efficiently exported out of the system via the Norwegian Deep Channel, contributing directly to the carbon budget of the

North Atlantic Ocean. Due to bathymetry, the North Sea is generally separated into a shallow mixed southern region, which acts as a CO_2 source, and the deeper stratified northern region, which acts as a significant CO_2 sink, taking up an estimated 8.5 Tg C yr^{-1} (Thomas et al. 2004, 2005; Salt et al. 2016).

Data sets

FerryBox measurements

A flow-through FerryBox (Petersen 2014) has been operated between Cuxhaven, DE and Immingham, UK since 2006, initially on board the TorDania (DFDS Seaways, Copenhagen DK) cargo vessel (CV), and after 2010, on board the CV Hafnia Seaways. One trip lasts for about 20 h. For this study, oceanographic data were collected via a FerryBox installed onboard the CV Hafnia Seaways (DFDS). The Hafnia has two main routes defined as the north and south route in Fig. 1. Sometimes the ship veered slightly further south or further north, depending on weather or ship traffic (Fig. 1). In 2017, the Hafnia Seaways traveled predominantly along the main north route, especially during the summer. However, by combining all south routes into one data set, it was possible to obtain a relatively complete time series along the south routes as well. The few (< 5) northern-most routes (Fig. 1) were not used in this study.

In 2017, while underway, the FerryBox measured continuously (every 10 s) a number of oceanographic parameters: temperature and salinity (Falmouth Scientific [FSI], Cataumet, Massachusetts and Teledyne Instruments, Poway, California, U.S.A.); dissolved oxygen (DO; Aanderaa optode, Xylem Analytics, Germany); chlorophyll fluorescence (Chl, ECO FLNTU, Seabird Scientific, U.S.A.); pH (Meinsberg pH glass electrode, Xylem Analytics, Germany); partial pressure of carbon dioxide (pCO_2, CONTROS HydroC CO_2 FT, Kongsberg Maritime Contros GmbH, Kiel, Germany), and chromophoric dissolved organic matter (CDOM, TriOS MicroFlu, Rastede, Germany). The regions near the two ports, 0.1°W–0.5°E and 8.0–8.7°E, were excluded from all data plots, so that any influence from the ship being in port, including cleaning cycles, was disregarded. Routine service was done on the Hafnia every 3–6 weeks, and consisted of replacing or calibrating the pH electrodes, collecting samples for Winkler titrations and/or replacing the DO optodes, cleaning the CDOM and chlorophyll fluorometers, or any additional maintenance of the other instruments and the FerryBox flow-through system.

Dissolved oxygen

Between 2016 and 2017, one optode was used and 12 discrete samples (in duplicates or triplicates) for Winkler titration were collected when the ferry was in Cuxhaven. The average differences between the Winkler titrations and the optode measurements were -5.9 ± 3.1 μM and $-2\% \pm 1\%$ saturation, with no significant drift. Therefore, no correction was applied to the DO measurements for this period. Rarely the optode was affected by (micro) bubbles caused by rough seas. One way that these bubbles' influence could be tracked was via side-by-side plots of DO and turbidity measurements. Since the major biological signals were not affected, these "noisy" measurements were not removed from the DO data.

CDOM fluorescence

The same CDOM sensor was used between December 2015 and November 2017. Last calibrated by TriOS at the end of 2013, the instrument absolute measurements were most likely inaccurate (recommended interval for recalibration by the manufacturer is 2 yr after continuous use). However, regular maintenance (cleaning the optics every 1–2 months) and solid calibration checks were used to track for any drift. Supporting Information Fig. S1 revealed that the instrument was reading higher than expected concentrations, but the offset was stable during 2016 and 2017. Two outliers were not included in the calculation of the mean and standard deviations of the offset. Based on this analysis, the CDOM measurements probably correctly captured the 2017 environmental fluctuations in dissolved organic matter (DOM), but their absolute values were inaccurate. Therefore, in this study, we refer to the CDOM values as μg L^{-1}, as they are reported, but their accuracy is questionable.

pCO_2

Two CONTROS HydroC CO_2 sensors were used onboard the Hafnia Seaways in 2017. The first one was installed on 17 October 2016 and removed in July as a result of a major water leak. The second one was installed on 11 July 2017 and was removed in January 2018. The pCO_2 data (Supporting Information Fig. S2a) were corrected for "zero" (blank) measurements, which can account for instrument drift. The zero values (20–30 μatm, Supporting Information Fig. S2b), were measured every 6–8 h by bypassing the membrane, where equilibration takes place, and instead recirculating air through a CO_2 scrubber, which removed CO_2. This allowed for drift tracking of the infrared (IR) sensor, which was minimal in 2017, in both instruments. The data in between the zero measurements were interpolated, so that a time series of zero values was subtracted from the pCO_2 measurements. A second step in the pCO_2 correction required the removal of data affected by the flush cycle after each zero measurement. The time that the HydroC CO_2 instruments need for full equilibration depends on the instrument configuration and environmental conditions.

The CONTROS HydroC CO_2 instrument has been found to agree well with independent pCO_2 measurements in the North Sea. The fugacity of CO_2 (fCO_2) calculated from pCO_2 and temperature measurements from another cargo vessel instrumented with a FerryBox, the CV Lysbris Seaways, were compared to fCO_2 calculated from nearby cross-over measurements made by the highly accurate method of headspace equilibrator with an IR detector by the Centre for Ecosystem Fisheries and Aquaculture Science (CEFAS) (Kitidis et al. 2018). According to SOCAT guidelines (Olsen et al. 2015), cross-overs

were defined as measurements within a maximum distance of 80 km of one another, where an algorithm of both space and time is used; in the North Sea coastal waters, Kitidis et al. (2018) used a more conservative distance of 40 km instead, and found 91 cross-overs between the Lysbris measurements and the CEFAS data. The slope of the line of the comparison was statistically indistinguishable from one, with a residual of 16.7 μatm, which indicated that the two data sets were comparable, despite the time and space differences between sample measurements. In coastal surface waters, where gradients in biologically mediated parameters like pCO_2 vary spatially and temporally (even over a day) by more than an order of magnitude (Thomas et al. 2004; Tortell et al. 2014), this difference is small.

Total alkalinity

TA was measured using the CONTROS HydroFIA TA analyzer (Kongsberg Maritime Contros GmbH, Kiel, Germany), starting in March 2017. In the flow-through setup (Supporting Information Fig. S3), sample water, diverted from the main flow, was filtered through a 0.2 μm cross-flow filter. The filtered sample water was collected in a reservoir (~ 200 mL long tube), connected to the TA system intake (Supporting Information Fig. S3). Timing of the sample intake and measurement frequency were tested during the first 2 months of deployment; following these tests, it was decided that sampling every 10 min was sufficient to capture TA patterns along this route. Reagents made in the laboratory (0.1 N HCl and Bromocresol green indicator dye) were replaced every 6 weeks. After each reagent change, the instrument was calibrated using a certified reference material (CRM) provided by Andrew G. Dickson's laboratory. On 2 d (15 May 2017 and 22 August 2017), the calibration onboard the Hafnia Seaways was not successful, and the instrument measurements after calibration were lower than the CRMs. The TA record was corrected by adding 105 μmol kg^{-1}, to all samples between 15 May 2017 and 07 June 2017 and 84 μmol kg^{-1} to all samples between 22 August 2017 and 25 September 2017. The offsets were calculated using the difference between expected and measured value of CRM before the next calibration. A short-term drift (3–4 samples) in the TA measurements was observed every time the Hafnia started a cruise, after being in port for more than 6 h. This drift took place within the port regions mentioned above, and thus did not affect the data used in this analysis.

pH

The pH glass electrode was regularly calibrated during maintenance of the FerryBox against certified buffer solutions based on NBS scale (Metrohm, Switzerland, order no. 6.2307.230) at pH of 7.0 and pH of 9.0. The major drift was observed in the offset at pH of 7.0 (zero point) whereas the calibration slope (mV per pH unit) changed only slightly. If the drift was too large, the electrode was replaced. In order to remove the jumps in measured pH values after each field calibration, the offset at pH 7 and the slope of the calibration was correlated against the respective time. There was a strong linear correlation between the intercept change and time, with a typical drift of about 30–35 mV yr^{-1} or 0.04–0.05 pH units per month (Supporting Information Fig. S4). Using the equation of the linear regression of a certain pH probe, the actual offset at pH of 7.0 and the actual slope were calculated for each recorded cell voltage (normalized at 25°C) and the actual pH value was recalculated according to Eq. 1:

$$\mathrm{pH} = 7 + (U_{T25} - a)/b \quad (1)$$

where U_{T25} is the measured cell voltage (mV) normalized at T = 25°C, a the offset at pH of 7.0 (mV), and b the slope (mV per pH unit).

Discrete samples: Total dissolved inorganic carbon and TA

Discrete samples onboard the Hafnia Seaways were collected autonomously via an ISCO sampler, during three cruises (n = 5–14: 28 March 2017, 20–21 April 2017, and 30–31 July 2017) on the route from Immingham to Cuxhaven. Dissolved inorganic carbon (DIC) and TA subsamples were subsequently collected, and fixed with saturated mercuric chloride solution, as soon as the Hafnia came to port. Therefore, the ISCO sample water remained unfixed and unfiltered (refrigerated and in the dark) after collection for up to 24 h. The DIC samples from the Hafnia were collected in either 100 mL BOD bottles or 500 mL borosilicate glass flasks (used also for TA analysis). All DIC samples were measured by an AIRICA DIC analyzer (Marianda, Kiel, Germany), and CRMs were used as standards, measured regularly during sample analysis (Dickson, Scripps Institution of Oceanography). Uncertainties were ± 2–4 μmol kg^{-1}.

Between 08 July 2017 and 25 July 2017, discrete samples were collected manually from a FerryBox onboard the RV Heincke (Fig. 2a), and were compared to measurements from a second HydroFIA TA instrument. These samples, collected in 500 mL Duran bottles, were fixed immediately after collection, following methods described by Dickson et al. (2007). They were measured using a VINDTA DIC/TA analyzer (Marianda, Kiel, Germany) coupled to a UIC 5015 CO_2 coulometer (UIC, Joliet, Illinois, U.S.A.) according to SOP2 and SOP3b in (Dickson et al. 2007). CRMs for DIC and TA were measured regularly during the analysis. Uncertainties for DIC were ± 2–4 μmol kg^{-1} and for TA were < 1 μmol kg^{-1}. Separate DIC samples were also collected in 25 mL scintillation vials, and were analyzed on the AIRICA DIC analyzer according to the method described in the above section. The measured DIC values were then compared to DIC values, calculated based on HydroFIA TA and HydroC CO_2 underway measurements, using the dissociation constants from Millero et al. (2006), and CO2SYS program for MATLAB (van Heuven et al. 2011).

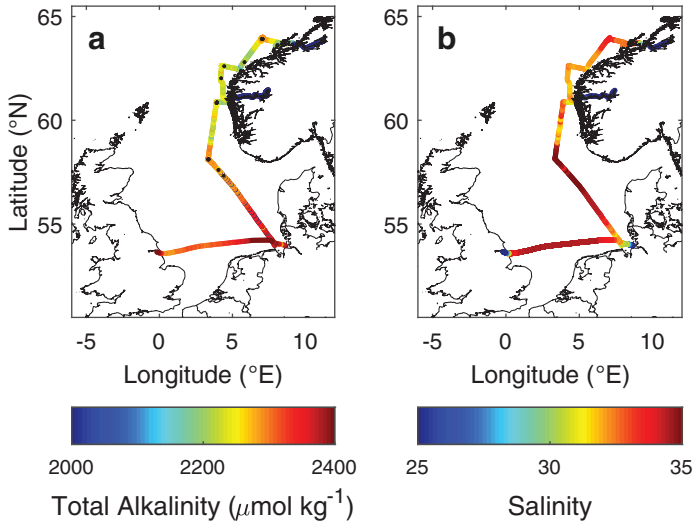

Fig. 2. (**a**) Total alkalinity and (**b**) salinity onboard the Hafnia Seaways between Cuxhaven and Immingham, 11 July 2017, and along a RV Heincke research cruise in the North Sea, 8–25 July 2017. The black dots (**a**) signify the position of the discrete sampling.

Results

Methodological challenges

Sampling onboard the RV Heincke allowed for direct comparison of discrete TA samples and HydroFIA TA measurements (Fig. 2). The comparison was robust, with slope of 1.031 (± 0.284), intercept of −76.33 (± 640.8) μmol kg^{-1}, and R^2 of 0.72 (n = 7). The root mean square error (RMSE) of the fit, 18 μmol kg^{-1}, was smaller than the expected instrument accuracy of 25 μmol kg^{-1}, including the sampling/matching error. TA measurements from the two HydroFIA TA instruments (RV Heincke and CV Hafnia Seaways) were very similar (Fig. 2a), as were the salinity measurements (Fig. 2b). Large changes in water mass characteristics were captured in differing TA (Fig. 2a) and salinity (Fig. 2b) distributions: in the German Bight, TA was highest north of the Wadden Sea, despite the lower salinity, while in the Norwegian Deep Channel, located along the Norwegian coast (57–62°N, 3–5°E), TA was lower where salinity was low. This suggests that, even though the absolute value of the TA may be slightly offset (on average by ± 18 μmol kg^{-1}), TA concentration changes within the North Sea regions were captured by the HydroFIA TA.

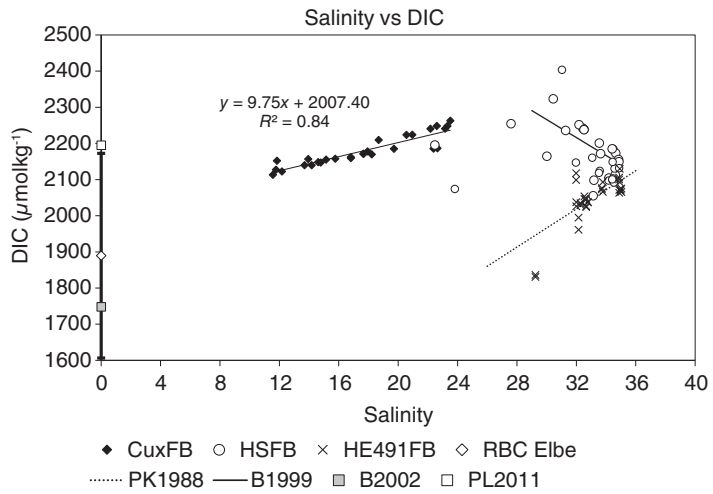

Fig. 3. Salinity vs. DIC (μmol kg^{-1}) in the nearshore and coastal waters of the North Sea. Water masses are separated into Elbe estuary (diamonds (CuxFB), measured at Cuxhaven, DE over several tidal cycles between 25 April 2016 and 15 May 2017); German Bight and South North Sea (open circles (HSFB), measured from Hafnia Seaways samples collected between Cuxhaven, DE and Immingham, UK); central and northern North Sea and Norwegian Deep (samples from RV Heincke 491 cruise [HE491FB], shown in this figure). As a reference, we show DIC relationships to salinity measured by the River Basin community Elbe (FGG Elbe 2018) (RBC Elbe), Pegler and Kempe (1988) (PK1988), Brasse et al. (1999) (B1999), Brasse et al. (2002) (B2002), and Pätsch and Lenhart (2011) (PL2011).

The calculated DIC values, based on underway TA and pCO_2 measurements, compare well to DIC measured in the laboratory (Supporting Information Fig. S5). Two regressions were generated: the first one with a slope of 0.963 (± 0.076), and an intercept of 82.30 (± 162.2) (R^2 = 0.93, df = 12, RMSE = 13 μmol kg^{-1}), was based on DIC samples collected on 20–21 April, 2017 (n = 6), and 30–31 July (n = 14). Six samples in this regression were found to be outliers, based on stepwise elimination of standardized residuals, whose absolute values were > 1. The second regression, with a slope of 0.878 (± 0.203), and an intercept of 214.2 (± 453.8) (R^2 = 0.86, df = 3, RMSE = 6 μmol kg^{-1}), was based on samples from 28 March, 2017 (n = 5). The calculated DIC differed on average by < 15 μmol kg^{-1} from the DIC measured in the laboratory.

We used discrete DIC samples, collected between 2016 and 2017 from three FerryBoxes (Cuxhaven [CuxFB], CV Hafnia Seaways [HSFB], and RV Heincke [HE491FB]), to characterize the regional water masses in the German Bight and the North Sea, and thus compare our measurements to previous studies (Fig. 3). The Elbe estuary (from tidal sampling at Cuxhaven) shows that DIC increased with salinity, with a robust linear regression (R^2 = 0.84). Samples from CV Hafnia Seaways deviated from another linear relationship much more, although they varied inversely with salinity. Their distribution was close to the relationship found by Brasse et al. (1999) for the German Bight and the transition zone between the Wadden Sea and the coastal waters (R^2 = 0.87). DIC samples collected in the open North Sea, and the Norwegian Trench (Fig. 2), have yet a different relationship to salinity, which fits the one described by Pegler and Kempe (1988) for the Skageraak and the Norwegian Deep. Therefore, DIC samples collected from three FerryBox systems agreed well with previous studies in the North Sea, and specifically in the German Bight.

Spatial and temporal patterns: North vs. south routes

The lowest salinities along both routes were measured in late spring-early summer (April–July) east of 6°E (Fig. 4a), suggesting the influence of local rivers, like the Elbe, Ems, and

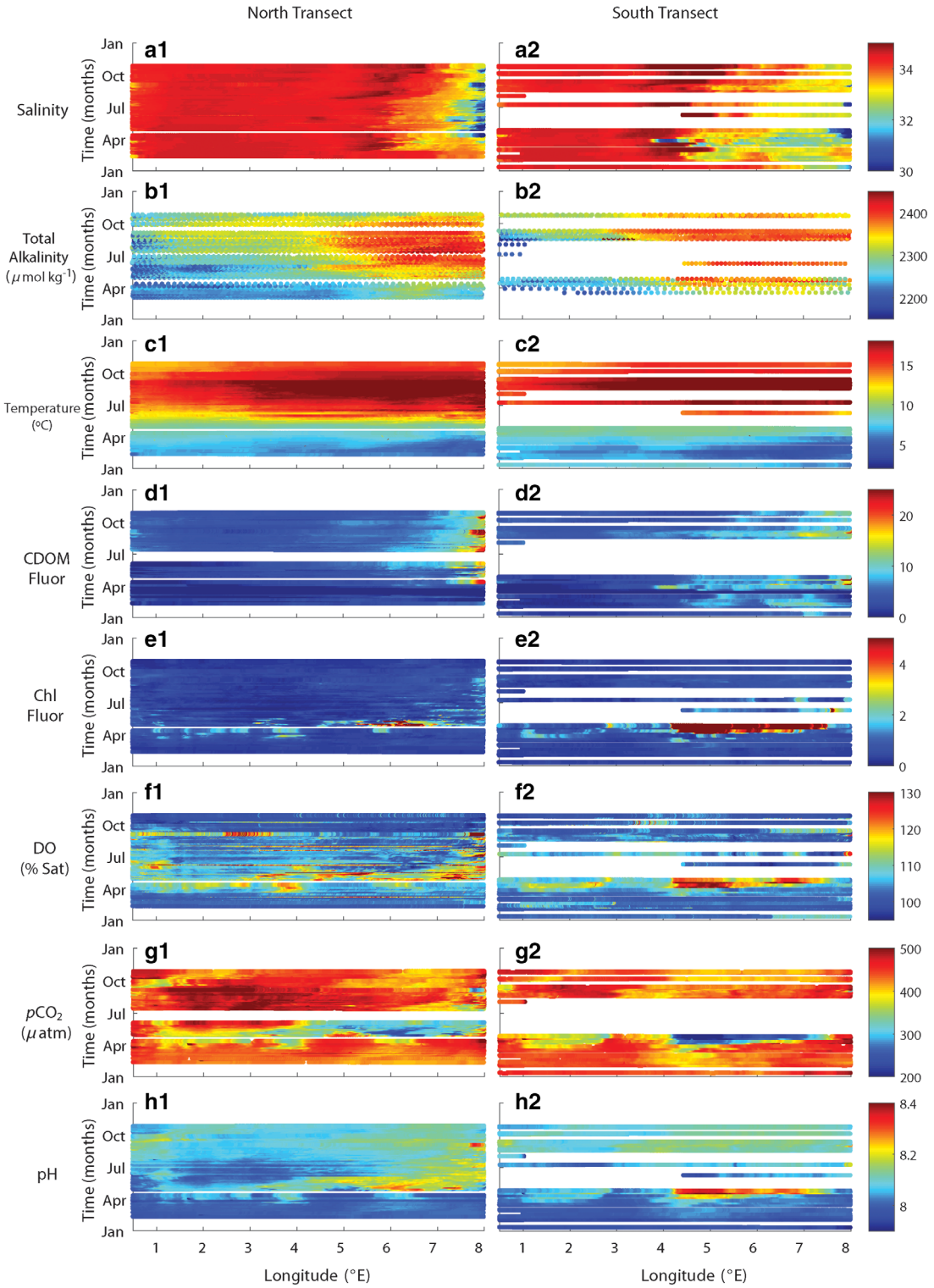

Fig. 4. (**a**) Salinity, (**b**) TA (μmol kg^{-1}), (**c**) temperature (°C), (**d**) CDOM fluorescence (μg L^{-1}), (**e**) Chl fluorescence (μg L^{-1}), (**f**) DO (% saturation), (**g**) (pCO_2 (μatm), (**h**) pH (NBS) measured along the north (marked with 1) and south (marked with 2) routes (Fig. 1) in 2017.

the tributaries of the Rhine River (Fig. 1). Along the north route (Fig. 4a1), the lowest salinities (< 33) were observed between April and October, with defined periods of low salinity outflows. Along the south routes (Fig. 4a2), closer to the Wadden Sea, the lowest salinities were observed in early spring (February–May), when surface waters east of 4.5°E were

considerably fresher (< 33) than adjacent waters to the west (> 34). The highest salinities (> 34) were measured around 4°E along the south route (Fig. 4a2), and 5–6°E along the north route (Fig. 4a1), delineating a strong gradient in an area of about 1° longitude. Salinity west of 5°E in the north and 3°E in the south routes was relatively high and stable, around 34, with the exception of the coastal waters near Immingham (west of 1°E), where salinities decreased (< 34).

TA (Fig. 4b) did not follow the pattern of salinity distribution (Fig. 4a): seasonally, TA increased along the entire transect and particularly north of the Wadden Sea (east of 4°E, Fig. 1) from < 2250 μmol kg^{-1} in March to > 2400 μmol kg^{-1} in August–September. There was also a significant difference between the waters west and east of 4°E: in the east, TA was 100–200 μmol kg^{-1} higher (Fig. 4b1,b2). There was also a spatial and seasonal variation in the TA between the north (Fig. 4b1) and south (Fig. 4b2) routes: generally TA was higher in proximity to the Wadden Sea. Along all longitudes, there was a general pattern of increasing TA, reaching a peak in August–September and tapering off in October.

Temperature increased seasonally (Fig. 4c), reaching a maximum in August–September. In the summer, there was a slight gradient of increasing temperature from west to east (12–15°C near Immingham to 15–20°C near Cuxhaven). The seasonal trend between the north (Fig. 4c1) and south (Fig. 4c2) routes was similar, except in the winter, when waters near the Wadden Sea and the western part of the southern North Sea (SNS) remained colder.

The distribution of CDOM fluorescence (Fig. 4d), which could be used as a proxy for dissolved organic carbon (DOC) variations (Painter et al. 2018), was highest in the summer and the fall, and lowest between January and May. This seasonal cycle in CDOM was observed in both the north and south routes, independent of longitude. The increase in CDOM fluorescence over the course of the year could also be observed in a salinity vs. CDOM plot (Supporting Information Fig. S7a). In addition, there was a distinct east-west gradient (Supporting Information Fig. S7), with highest CDOM east of 4°E along the south route (Fig. 4d1), and east of 5°E along the north route (Fig. 4d2), closely related to salinity fluctuations (Supporting Information Fig. S7a). The overall highest CDOM values (> 20 μg L^{-1}) were observed along the north route, east of 7.5°E, and coincided with low-salinity outflows (most likely from the Elbe and Ems rivers). CDOM increased with TA as well (Supporting Information Fig. S7b).

The biogeochemical parameters directly affected by local primary production and respiration (chlorophyll *a* [Chl *a*] fluorescence, oxygen, pCO_2, and pH; Fig. 4e–h) had a strong seasonal, as well as a weaker north-south and east-west gradient. In 2017, highest Chl *a* fluorescence (Fig. 4e) was observed in April–May, with a more pronounced signal along the south route, and east of 4°E. This suggests an increase in the produced biomass in the SNS, as a result of the spring bloom. High primary production in the spring (April–May) coincided with the time of high fluorescence based on DO (Fig. 4f, 120–130% saturation), low pCO_2 (Fig. 4g, 200–350 μatm), and high pH (Fig. 4h, 8.2–8.4) measurements. In the summer, along the north route (1.5–7°E), surface waters were characterized by lower DO (Fig. 4f1, ~ 100% saturation), high pCO_2 (Fig. 4g1, > 400 μatm), and lower pH (Fig. 4h1, 7.9–8.1). Along the south route, the lack of measurements between May and August (Fig. 4f2, g2, h2) prevented from drawing a definitive conclusion, but the few available DO measurements suggest that the water column was slightly more productive. The highest primary production was observed east of 4°E, and along the south route, closer to the Wadden Sea. In June–July, primary production was still high east of 4°E, and particularly in the 6–8°E regions. This was evident by low pCO_2 (Fig. 4g1) and high pH (Fig. 4h1). In comparison, DO was evenly supersaturated along the entire transect (DO > 100% saturation, Fig. 4f1). This suggests that, north of the Wadden Sea, surface waters were productive in the spring–summer season, even though summer respiration rates were probably higher than production rates.

Spatial and temporal patterns: Focus on nearshore to coastal gradient

When plotting the time series along a narrow longitude range (0.2°, Fig. 5), it becomes clearer that on top of the seasonal cycle of increasing TA, there are specific regional fluctuations, along the east-west gradient. In the west (~ 2°E), where salinity was high (> 34, Fig. 5a1), TA was evenly distributed between the north and south routes (Fig. 5b1) up to the end of August. After, during the fall, some southern readings were lower. TA increased seasonally from ~ 2200 μmol kg^{-1} in March–April to ~ 2350 μmol kg^{-1} in September–October. Overall, CDOM increased slightly seasonally (Fig. 5c1, from ~ 0 μg L^{-1} in February–March to ~ 5 μg L^{-1} in September–October), but there was no difference between the north and south routes. A proxy for primary production, the lowest pCO_2 (Fig. 5d1, < 350 μatm), was observed in early spring, around March. In the southern-most routes, the chlorophyll bloom was delayed by about 1 month. After a relatively short productive period, pCO_2 became high (~ 450 μatm) by May.

At longitude 4.8–5.0°E (Fig. 5), the Hafnia traveled near the Dutch Wadden Sea along the south route, and 0.5° to the north along the north route. Salinity along the north route was uniformly high (> 34), suggesting a characteristic of the open North Sea water, either from the North Atlantic inflow through the English Channel, or from the central parts of the North Sea. While TA along the north route varied, with a higher rate of increase in May–June, and then in August (Fig. 5a2), salinities remained high (Fig. 5b2). Along the south route, lower salinities suggest the influence of the Rhine River/Wadden Sea outflow. Here, a large increase in TA (Fig. 5a2) was observed in April–May, when salinities were increasing (Fig. 5b2). However, TA continued to increase to a maximum in August–September, independent of salinity.

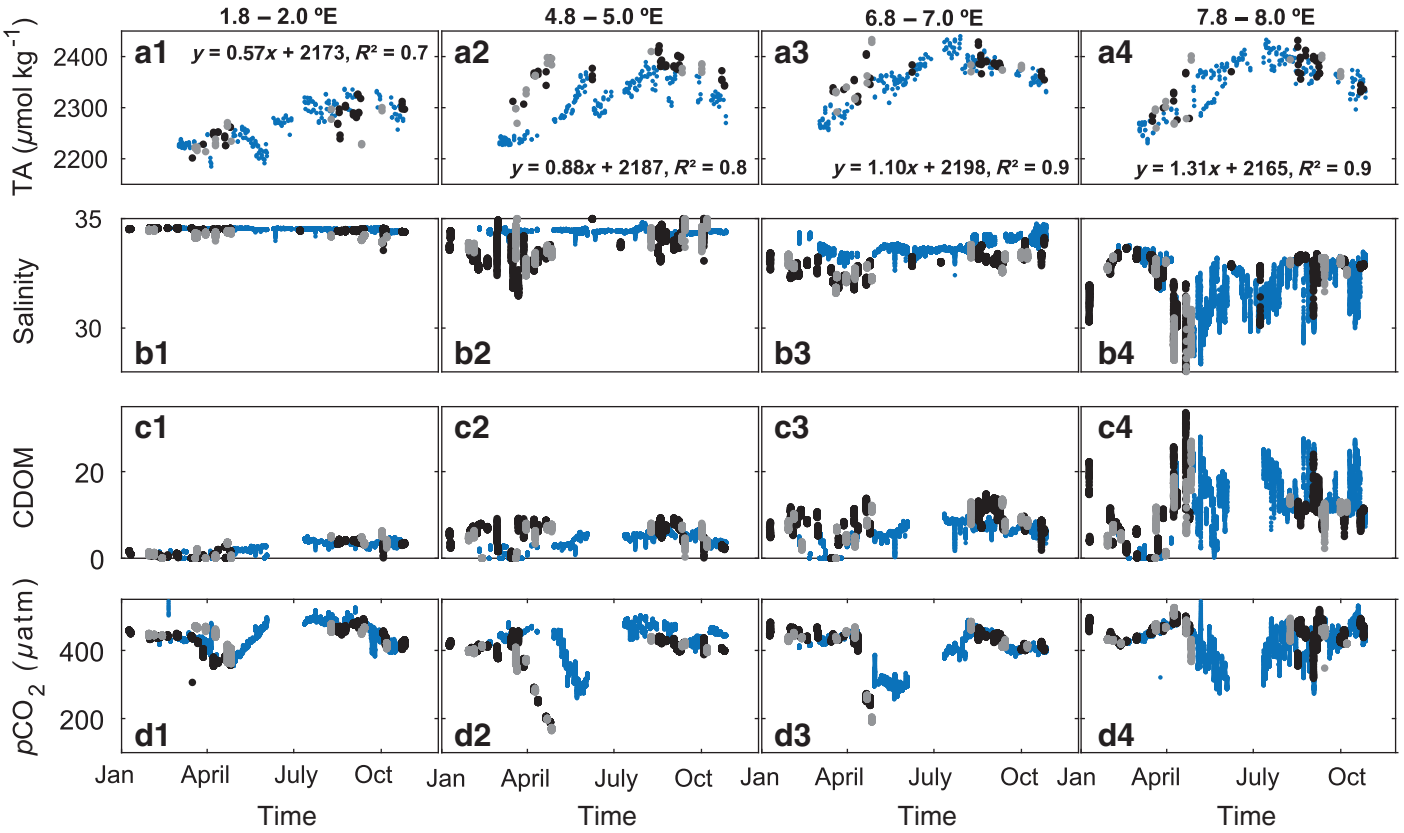

Fig. 5. (**a**) Total alkalinity (TA, μmol kg^{-1}), (**b**) salinity, (**c**) colored dissolved organic matter fluorescence (CDOM, μg L^{-1}), (**d**) partial pressure of carbon dioxide (pCO_2, μatm). Indices next to each letter stand for regions of longitude along the Hafnia seaways route: 1 = 1.8–2.0°E, 2 = 4.8–5.0°E, 3 = 6.8–7.0°E, 4 = 7.8–8.0°E. Colors indicate the north (blue) and south routes (black and gray), as shown in Fig. 2a. Also plotted are fits relating the daily (interpolated) TA to time, so that the slopes and intercepts (Table 1) of the seasonal (March through July–September) TA increase are obtained for each longitude range (*see* Supporting Information Fig. S7).

CDOM differed: in the south, CDOM was higher, coincident with lower salinities, while in the north, there was a pronounced seasonal CDOM increase (Fig. 5c2). The lowest pCO_2 in the south took place about a month (April) before the lowest observed pCO_2 in the north (May–June), and these troughs coincided with respective increases (peaks) in TA (Fig. 5a2). While in the spring, there was a large difference between the north and south TA concentrations, this difference disappeared by September–October, when TA concentrations along both routes were uniformly high (Fig. 5a2).

To the east, at longitude 6.8–7.0°E (Fig. 5), TA increased from about 2250 μmol kg^{-1} in March to 2400 μmol kg^{-1} in August along the north route (Fig. 5a3). In the south, TA was higher by up to 50–100 μmol kg^{-1}, and this difference was particularly striking in the spring to early summer. The only exception was several measurements along the south route, which coincided with TA ranges from the north route. Based on salinity (Fig. 5b3), it can be deduced that these back to back south measurements of differing TA were made during different stages of the tide. This suggests that there is a strong gradient between the Wadden Sea and the adjacent North Sea, and there can be up to 100 μmol kg^{-1} difference in TA over a tidal cycle. Due to a lack of summer measurements along the south transect, it was difficult to say how long the difference between the nearshore and the coastal waters was maintained, but by August–September, it seems to have disappeared. Generally, CDOM varied inversely to salinity (Fig. 5c3, Supporting Information Fig. S7), with lower salinity and higher CDOM along the south route. The spring bloom in this region started later than the western regions, but the north and south routes had similar pCO_2 patterns, differing only slightly in April.

A seasonal TA maximum in August was also evident at longitude of 7.8–8.0°E (Fig. 5), this time observed in both the north and south routes, since at this longitude, the Hafnia passed through the same position along both routes. At this location, the ship measured two different water masses carrying distinctly different TA concentrations depending on the stage of the tide. The tide-dependent TA difference occurred from March until June–July, but was largest (~ 100 μmol kg^{-1}) when salinities were lowest (April–May, Fig. 5b4). At this longitude, CDOM was overall higher and more variable (Fig. 5c4, > 15 μg L^{-1}) than the other regions. The time of the spring

Table 1. Intercept, slope, assumed depth and average temperature and density, and calculated TA flux, depending on region, based on longitude range.

Longitude (°E)	Intercept (μmol kg^{-1})	Slope (μmol kg^{-1} d^{-1})	Depth (m)	Temperature (°C)	Density (kg m^{-3})	TA flux (mmol m^{-2} d^{-1})
1.8–2.0	2172.8 ± 5.1	0.57 ± 0.03	20	15	1028	11.7 ± 0.6
4.8–5.0	2174.0 ± 6.6	0.88 ± 0.05	20	15	1027	18.0 ± 1.0
6.8–7.0	2198.4 ± 4.2	1.10 ± 0.03	20	15	1026	22.7 ± 0.6
7.8–8.0	2165.3 ± 5.9	1.31 ± 0.04	20	15	1024	26.8 ± 0.9

bloom occurred later in the year (lowest pCO_2 in June, Fig. 5d4), whereas during most of the spring period, when salinity was low, pCO_2 was high, reflecting the Elbe influence.

Seasonal TA generation

The data collected along the north route can be considered as a proxy for the characteristics of the surface waters in the southern regions of the SNS, as defined by Brenner et al. (2016). Linear regressions, fit to the daily SNS TA increase (interpolated) between March and September, gave rates of TA increase (flux) during the spring–summer season (Fig. 5a1–a4; Supporting Information Fig. S8). Despite the TA variability caused by local changes in biological processes and tidal dynamics, all fits had $R^2 > 0.5$. In the western regions (1–5°E), the increase in TA lasted slightly longer (~ 1 month). Nonetheless, the slope increased and even doubled between the western SNS (0.57, Fig. 5a1, 1.8–2.0°E) and the German Bight, east of 6°E (1.10–1.31, Fig. 5a3,a4). Using an estimated SNS water column depth of 20 m, a density of 1024–1028 kg m^{-3}, and an average temperature of 15°C (Table 1), calculated TA increases in SNS surface waters ranged from 12.3 mmol m^{-2} d^{-1} to 26.6 mmol m^{-2} d^{-1}, depending on longitude.

Discussion

Data integrity

The flow-through setup described in this study, where a TA analyzer was combined with a FerryBox, was used successfully to measure surface TA on moving platforms in coastal waters. Direct comparisons to manually collected samples measured in the lab, revealed that HydroFIA TA measurements were accurate (according to the expected manufacturer accuracy of 25 μmol kg^{-1}). Additional comparison between measured DIC (from an ISCO auto-sampler) and calculated DIC (from underway HydroFIA TA and HydroC CO_2 measurements) served as an independent check of the HydroFIA TA performance. This method had the drawback of no immediate fixing of the ISCO samples, as recommended by Dickson et al. (2007). This could explain why, out of 20 samples, 6 were outliers, located at the beginning or the end of the cruise from Immingham to Cuxhaven (Supporting Information Fig. S6a). The samples near Immingham were left without mercuric chloride the longest, therefore their DIC concentrations were most likely affected by gas exchange and biological processes. At the end of each cruise, near Cuxhaven, the ship entered waters with lower salinities (Supporting Information Fig. S6b), and variable pCO_2 (Supporting Information Fig. S6c) and TA (Supporting Information Fig. S6d): a dynamic environment, where a multitude of factors could influence the equations used by the HydroFIA TA, and the calculated DIC. Nevertheless, the absolute differences between measured and calculated DIC for all samples of the April–July fit (Supporting Information Fig. S5) were less than 25 μmol kg^{-1} (Supporting Information Fig. S6a, average 12 ± 7 μmol kg^{-1}), with an RMSE of 18 μmol kg^{-1}. The smaller slope (~ 0.9, Supporting Information Fig. S5) of the second fit generated by the 28 March samples could be explained by the early testing of the HydroFIA TA, but these TA measurements still produced calculated DIC comparable to the measured values (RMSE = 6 μmol kg^{-1}). This difference can be critical, so one must be careful when interpreting the data. Based on these comparisons however, we find that the HydroFIA TA measured accurately the TA in surface waters of the North Sea.

The comparison of measured DIC (collected manually or via an ISCO sampler) to previous studies and historical data (Fig. 3) indicates that the above check methods can be used effectively to distinguish between water masses in the North Sea and the German Bight. The intercept of 2007.4, based on the Cuxhaven FerryBox samples, was less than the Elbe River DIC concentration from Pätsch and Lenhart (2011), 2195 μmol kg^{-1}, but larger than the concentration measured in the upper estuary (salinity = 0) by Brasse et al. (2002), 1748 μmol kg^{-1}. In fact, DIC (originally in mg L^{-1}), measured by the River Basin Community Elbe (FGG Elbe 2018) at Seemanshöft station (~ 100 km upstream from Cuxhaven), varied seasonally (1992–2016), with an average of 1889.5 ± 283.0 μmol kg^{-1} (Fig. 3). This seasonal variation can explain the spread in historical measurements, and our measurements fall within the relationships to salinity described by previous studies, which indicates their robustness. Even though the CV Hafnia Seaways samples deviated from the linear relationship found by Brasse et al. (1999), these deviations can be explained by the proximity of the Wadden Sea, which was found to be a significant source of DIC. Therefore, this summary figure (Fig. 3) can be used as an independent verification of the discrete sample collection methods used in this study.

Finally, one aspect that could influence the HydroFIA TA measurements is the variability of organic matter (Kim et al. 2006;

Hernández-Ayon et al. 2007), which is not accounted for in the TA definition by Dickson (1981). Organic alkalinity constitutes a minor fraction of TA, but it has been shown to drastically influence the calculated values of pH and pCO_2 (Kuliński et al. 2014). This suggests that the acid-base properties of DOM must be included when calculating the carbonate system parameters in systems heavily influenced by DOM inputs (Gustafsson et al. 2014; Kuliński et al. 2014). DOC in the North Sea is generally low (80–120 μmol L^{-1}), and the area of the German Bight, and Rhine River outflow has some of the highest concentrations ranging between 100 μmol L^{-1} and 160 μmol L^{-1} (Painter et al. 2018). These concentrations are low compared to the Baltic Sea region (Kuliński et al. 2014), where organic alkalinity was found to be important. The Dutch Wadden Sea has been found to have higher concentrations only in May–June, 300–400 μM (Cadee 1982), corresponding to a potential organic TA fraction of about 30 μmol kg^{-1} (Kuliński et al. 2014). Since the North Sea coastal waters have lower DOC concentrations, we can expect that the error in TA measurements associated with organic TA is small (< 30 μmol kg^{-1}), and cannot account for the larger fluctuations discussed in this article. Moreover, CDOM, when used as a qualitative proxy for DOC variability, varied as a function of salinity (Voynova et al. 2017) (Supporting Information Fig. S6a). Since measured TA concentrations were decoupled from salinity, the influence of organic matter is probably minimal. Still, in future studies, the equation for calculating TA could be altered to include DOC and to verify this.

TA sources

There were several potential sources of TA to the study region that included river outflow, intertidal regions, and bottom sediments described in the following sections.

River outflow

The high-frequency measurements acquired in this study revealed several characteristics of TA in coastal waters that were used to identify possible TA sources. Seasonally, TA in surface waters of the German Bight and the SNS increased from spring to fall, and subsequently decreased through late fall, with a pronounced seasonal change of at least 100–150 μmol kg^{-1} (Fig. 5a). This seasonal TA cycle did not follow a similar salinity change, which suggests that it was independent of river inflow. Two major rivers, the Elbe and the Rhine, should be considered when verifying this. The Elbe, which discharges to the German Bight near Cuxhaven and influences coastal biogeochemistry (Hickel et al. 1993; Brockmann et al. 1999; Voynova et al. 2017), has an estimated TA of 2231 μmol kg^{-1} (Pätsch and Lenhart 2011). This is lower than the TA concentrations in the adjacent coastal region (Fig. 5a3,a4), which suggests that the Elbe is not a large TA source. In fact, Brasse et al. (2002) found lower TA in the upper Elbe estuary in April (1760 μmol kg^{-1}). The Rhine River tributaries had generally high TA (2580–3832 μmol kg^{-1}; Pätsch and Lenhart 2011; Schwichtenberg 2013) and could be a TA source, but TA loads were lowest between June and November (Pätsch and Lenhart 2011). The highest TA contribution from the Rhine is expected in January–April (Fig. 5b2), and thus river discharge could not have accounted for the observed seasonal TA increase in coastal waters. This is supported by Schwichtenberg (2013), who, based on a model, found that only 9% of the TA changes in the German Bight were caused by effective river loads.

Intertidal regions (Wadden Sea)

The seasonal TA change observed in this study is similar to the pattern attributed to the Wadden Sea by Thomas et al. (2009), except larger in magnitude. East of 4°E, the north-south gradient of increasing TA toward the nearshore regions, suggests that the Wadden Sea is a substantial source of TA to the adjacent coastal regions. This is supported by the TA difference of up to 100 μmol kg^{-1} in back to back FerryBox transects, likely moderated by the stage of the tide. This difference persisted over the spring–summer season and was best observed north of the Wadden Sea, between 6°E and 7°E, where a clear nearshore to coastal gradient was observed. In 2017, salinity measurements from the Spiekeroog tidal station (53°45′01.00″N, 7°40′16.30″E), located south of the Hafnia Seaways route were high (~ 30) (Badewien et al. 2017), and thus the salinity gradient between the Wadden Sea (6–7°E) inflow and outflow over a tidal cycle was minimal (1–2), as observed by the FerryBox (Fig. 5b3). TA tidal gradients were much more prominent (Fig. 5a3), therefore studying TA at the Spiekeroog station is a good next step for better understanding water mass characteristics, TA and carbonate dynamics in the Wadden Sea-North Sea region.

Other studies also support the idea of the intertidal regions as a source. Hoppema (1993) found that the Wadden Sea TA and DIC varied over a tidal cycle in May and in September, with the highest concentrations observed over the ebbing tide, suggesting that the tidal flats are a source of TA and DIC, specifically since pore-water TA is up to 20 times higher than typical coastal concentrations (Beck et al. 2008*a*). Based on coupled ^{222}Rn and pCO_2 observations, Santos et al. (2015) found that pore-water exchanges were equivalent to 1.1% of the tidal prism volume, and fluxes from pore water (1216–1811 mmol TA m^{-2} d^{-1}) represented a significant TA source of to the nearshore Wadden Sea water column. Therefore, the Wadden Sea intertidal flat sediments are a significant TA source to the overlying waters, and through tidal exchange (Santos et al. 2014), to the coast.

Bottom sediments (North Sea)

Another major TA source to surface waters could be bottom sediments (Brenner et al. 2016), especially valid in the regions where water column is well mixed (SNS). This could help explain the observed TA seasonal cycle in the regions west of 4°E, where the Wadden Sea has minimal influence. Brenner et al. (2016) found that bottom sediments in the SNS contributed on average about 6 mmol m^{-2} d^{-1} TA (0–21 mmol m^{-2} d^{-1}). This mean

flux is lower than the calculated fluxes from this study (12–27 mmol m^{-2} d^{-1}, Table 1), but it is comparable to the flux estimated west of 4°E (12 mmol m^{-2} d^{-1}). Near the Wadden Sea, TA fluxes doubled, which suggests that there was an additional source of TA, most likely from the intertidal flats. Similarly, Faber et al. (2014) found that tidal flats are active carbon pumps that transform organic matter into alkalinity, and this export to the coastal region is facilitated by tidal pumping. It should be noted that the estimated fluxes in this study only include the times of observed TA increases, and do not represent yearly estimates. The variable seasonal cycles also suggest that the TA sources are not constant, but instead, as assessed in the previous sections, vary depending on organic carbon fluxes, temperature variations, riverine inputs, and specific biogeochemical processes.

Mechanisms for seasonal TA change

The observed seasonal changes in TA could be explained by the following biogeochemical processes.

Organic matter cycling and temperature dependence

TA can change with calcium carbonate precipitation and dissolution, nutrient assimilation and remineralization by primary producers, nitrification, denitrification, and sulfate reduction (Wolf-Gladrow et al. 2007). One mechanism that could explain the seasonal cycle in TA is the coupling between organic matter production and remineralization, where the North Sea-Wadden Sea could play a major role. There is a net organic matter import from the North Sea to the Wadden Sea, estimated to be around 100 g C m^{-2} yr^{-1} (van Beusekom et al. 1999). This net import starts in early spring and continues through the summer (Postma 1981), and is probably highest during the spring bloom, when biomass is high (Figs. 4e, 5d). The Wadden Sea sediments function as a giant coastal filter, where organic matter from the North Sea and the overlying tidal flat area is captured and remineralized over time. Due to the advective flow characteristic of permeable sandy sediments, pore waters enriched in remineralized nutrients are actively released to the overlying water column (Beck and Brumsack 2012). This organic matter pool, is a substantial source of nutrients (Postma 1981; Grunwald et al. 2010), TA, and dissolved inorganic and organic carbon (Hoppema 1993; Santos et al. 2015) throughout the summer and fall. The tidal flats of the Wadden Sea therefore serve as a biogeochemical reactor, which facilitates organic matter remineralization and can generate a gradient in nutrients and TA from nearshore to coastal regions, mediated by the tidal flow. The time delay of when this organic matter is remineralized, likely related to temperature (Borges et al. 2017), and returned to the coast in dissolved form could account for the TA maximum observed in late summer–early fall.

In coastal waters, organic matter formation from autochthonous or allochtonous nutrient inputs could affect carbon cycling. In this study, the largest north-south TA gradients were observed at longitude of 5°E (Fig. 5a2), differentiating the Wadden Sea nearshore waters, influenced by the Rhine River, from the open North Sea waters in the north, influenced by the North Atlantic Sea flow through the English Channel (Otto et al. 1990). The pronounced TA increase was decoupled from salinity (Fig. 5b2), but coincided with the time of high-biological production (Figs. 4e–h, 5d2), when uptake of nitrate or nitrite in surface waters can increase TA (Stumm and Morgan 1981; Wolf-Gladrow et al. 2007). This region was particularly interesting, since the onset of the spring bloom in the north lagged the onset in the south by about a month. Despite the relatively short spring bloom, primary production had a pronounced effect on TA generation in both regions, and this should be considered when assessing TA dynamics.

Seasonally, an increase in temperature by 10°C can double reaction rates in natural waters (Chapra 1997). Depth-integrated sulfate reduction rates in permeable sediments can increase by a factor of 10 from winter to summer (Beck and Brumsack 2012), and microbially mediated sulfate reduction of organic matter in the Wadden Sea have been shown to increase by a factor of two in the spring and fall, and by a factor of 7 in the summer (Al-Raei et al. 2009). Therefore, a seasonal change of 15°C or more (Fig. 4c) would significantly increase the rates of the biogeochemical processes affecting TA, and can help explain the increased rate of TA production during the warm seasons. Coupled with the seasonal pattern in organic matter flux, and the seasonal temperature-dependence of organic matter remineralization, the TA flux from the Wadden Sea could increase seasonally, explaining the observed seasonal TA patterns in the North Sea.

Higher temperatures can enhance evaporation, which can subsequently drive an increase in salinity and TA (Schneider et al. 2007). Models have suggested that the average North Sea surface salinity in the 21st century will decrease by 0–0.3 psu (Schrum et al. 2016). Some models suggest that there may be a seasonal cycle of up to 0.075 psu, with lowest salinities in April and highest in October (Schrum et al. 2016). This fits the TA seasonal pattern observed here, but the expected TA change, based on a central North Sea and Atlantic Ocean relationship to salinity (Pegler and Kempe 1988), is equivalent to about 2 μmol kg^{-1}. Evaporation in the tidal flats of the Wadden Sea has been shown to increase salinity by 0.65 within 3.5 h, which suggests that during the warm months, tidal flats experience enhanced evaporation compared to other regions (Onken and Riethmüller 2010). According to Brasse et al. (1999), this salinity change for the German Bight and the adjacent nearshore regions (TA = −11.5 × salinity + 2719), corresponds to a TA change of about 7.5 μmol kg^{-1}. This could mean that higher evaporation compared to precipitation in the Wadden Sea can change TA, but is not enough to explain the observed coastal ranges over a tidal cycle (~ 100 μmol kg^{-1}) (Fig. 5a3).

Denitrification and sulfate reduction

Hu and Cai (2011*a*) suggested that denitrification plays a major role in net TA generation. Considering that denitrification

is only contributing to TA gain when nitrate used in this process is allochtonous (Hu and Cai 2011*a*), denitrification may be an important process for TA generation in the winter–spring, when nitrate from river influx is high. The Elbe could contribute to TA generation on the coast, since the major form of nitrogen in the estuary is nitrate, and its concentrations can vary seasonally by up to 200 μmol kg^{-1} (Schwichtenberg 2013). Major floods can be even more significant: after the 2013 Elbe flood, nitrate loading from the Elbe River increased up to 10-fold (Voynova et al. 2017).

Other studies found that in pore waters of anoxic sediments, the primary process affecting alkalinity was bacterial sulfate reduction (Berner et al. 1970). More recently, it has been suggested that sulfate reduction in sediments is an effective mechanism for remineralization of organic matter, significantly increasing TA in pore waters, and thus rendering bottom sediments as TA sources to the overlying water column (Brenner et al. 2016; Rassmann et al. 2016). In coastal systems influenced by terrestrial sources of iron, like streams and rivers, net TA production through the burial of reduced sulfur species as iron sulfides could be enhanced (Faber et al. 2014). This was observed in the Wadden Sea (Beck et al. 2008*a*,*b*), where sulfate and iron oxide reduction with the eventual formation of pyrite (burial) or hydrogen sulfide (degassing to the atmosphere at low tide) (Thomas et al. 2009) was the dominant pathway of anaerobic carbon remineralization.

Conclusions

In this study, the in situ measurement of TA was successfully implemented in a flow-through setup, in combination with a FerryBox. The TA measurements revealed that whereas alkalinity is typically considered a conservative parameter, in coastal systems, where carbon and nutrient fluxes are dynamic, TA can differ significantly (by up to 100 μmol kg^{-1}) between the nearshore and adjacent coastal regions. Properly accounting for net TA generation in these systems is of particular importance, as it may affect the carbon cycle and the coastal ocean's capacity to absorb atmospheric CO_2. Even though this study could not account for the sources of net alkalinity production in the coastal region, it demonstrated that there was a seasonal TA change of 100–150 μmol kg^{-1}. The seasonal change in TA was not due to riverine contributions, but instead was most likely related to seasonal organic matter production and remineralization in coastal and nearshore regions. Bottom sediments (Brenner et al. 2016) and the tidally coupled biogeochemical reactor between coastal (North Sea) and nearshore (Wadden Sea) regions are mediating this TA change, and the 4 months lag between the seasonal increase in TA and the peak in organic matter production and flux could be explained by the temperature-dependent remineralization of organic matter via both aerobic and anaerobic pathways. A more detailed study focused on the nearshore to coastal gradient and these processes could help disentangle the influences of aerobic remineralization vs. denitrification vs. sulfate reduction. In addition, a closer look on DOC production and fluctuations could help explain its influence on the TA measurements.

References

Al-Raei, A. M., K. Bosselmann, M. E. Böttcher, B. Hespenheide, and F. Tauber. 2009. Seasonal dynamics of microbial sulfate reduction in temperate intertidal surface sediments: Controls by temperature and organic matter. Ocean Dyn **59**: 351–370. doi:10.1007/s10236-009-0186-5

Anschutz, P., T. Smith, A. Mouret, J. Deborde, S. Bujan, D. Poirier, and P. Lecroart. 2009. Tidal sands as biogeochemical reactors. Estuar. Coast. Shelf Sci. **84**: 84–90. doi:10.1016/j.ecss.2009.06.015

Badewien, T. H., and others. 2017. Physical oceanography measurements in the tidal inlet between the islands Spiekeroog and Langeoog, Wadden Sea, North Sea, 2017–03. PANGAEA. doi:10.1594/PANGAEA.873900

Bauer, J. E., W. J. Cai, P. A. Raymond, T. S. Bianchi, C. S. Hopkinson, and P. A. Regnier. 2013. The changing carbon cycle of the coastal ocean. Nature **504**: 61–70. doi:10.1038/nature12857

Beck, M., and others. 2008*a*. Sulphate, dissolved organic carbon, nutrients and terminal metabolic products in deep pore waters of an intertidal flat. Biogeochemistry **89**: 221–238. doi:10.1007/s10533-008-9215-6

Beck, M., O. Dellwig, G. Liebezeit, B. Schnetger, and H.-J. Brumsack. 2008*b*. Spatial and seasonal variations of sulphate, dissolved organic carbon, and nutrients in deep pore waters of intertidal flat sediments. Estuar. Coast. Shelf Sci. **79**: 307–316. doi:10.1016/j.ecss.2008.04.007

Beck, M., and H.-J. Brumsack. 2012. Biogeochemical cycles in sediment and water column of the Wadden Sea: The example Spiekeroog Island in a regional context. Ocean Coast. Manag. **68**: 102–113. doi:10.1016/j.ocecoaman.2012.05.026

Becker, G. A., et al. 1999. Mesoscale structures, fluxes and water mass variability in the German Bight as exemplified in the KUSTOS-experiments and numerical models. German J. Hydrogr. **51**: 155–179.

Berner, R. A., M. Scott, and C. Thomlinson. 1970. Carbonate alkalinity in the pore waters of anoxic marine sediments. Limnol. Oceanogr. **15**: 544–549. doi:10.4319/lo.1970.15.4.0544

Borges, A. V. 2005. Do we have enough pieces of the jigsaw to integrate CO_2 fluxes in the coastal ocean? Estuaries **28**: 3–27. doi:10.1007/BF02732750

Borges, A. V., L. S. Schiettecatte, G. Abril, B. Delille, and F. Gazeau. 2006. Carbon dioxide in European coastal waters. Estuar. Coast. Shelf Sci. **70**: 375–387. doi:10.1016/j.ecss.2006.05.046

Borges, A. V., G. Speeckaert, W. Champenois, M. I. Scranton, and N. Gypens. 2017. Productivity and temperature as drivers of seasonal and spatial variations of dissolved

methane in the Southern Bight of the North Sea. Ecosystems **21**: 583–599. doi:10.1007/s10021-017-0171-7

Brasse, S., A. Reimer, R. Seifert, and W. Michaelis. 1999. The influence of intertidal mudflats on the dissolved inorganic carbon and total alkalinity distribution in the German Bight, southeastern North Sea. J. Sea Res. **42**: 93–103. doi:10.1016/S1385-1101(99)00020-9

Brasse, S., M. Nellen, R. Seifert, and W. Michaelis. 2002. The carbon dioxide system in the Elbe estuary. Biogeochemistry **59**: 25–40. doi:10.1023/A:1015591717351

Brenner, H., U. Braeckman, M. Le Guitton, and F. J. R. Meysman. 2016. The impact of sedimentary alkalinity release on the water column CO_2 system in the North Sea. Biogeosciences **13**: 841–863. doi:10.5194/bg-13-841-2016

Brockmann, U. H., and others. 1999. Seasonal budgets of the nutrient elements N and P at the surface of the German Bight during winter 1996, spring 1995, and summer 1994. German J. Hydrogr. **51**: 267–291.

Cadee, G. C. 1982. Tidal and seasonal variation in particulate and dissolved organic carbon in the western Dutch Wadden Sea and Marsdiep tidal inlet. Neth. J. Sea Res. **15**: 220–249.

Cai, W.-J., M. Dai, and Y. Wang. 2006. Air-sea exchange of carbon dioxide in ocean margins: A province-based synthesis. Geophys. Res. Lett. **33**: 1–4. doi:10.1029/2006GL026219

Carstensen, J., M. Chierici, B. G. Gustafsson, and E. Gustafsson. 2018. Long-term and seasonal trends in estuarine and coastal carbonate systems. Global Biogeochem. Cycles **32**: 497–513. doi:10.1002/2017GB005781

Chapra, S. C. 1997. Surface water-quality modeling. Waveland Press, Inc. Long Grove, IL, USA.

Chen, C.-T. A. 2002. Shelf-vs. dissolution-generated alkalinity above the chemical lysocline. Deep-Sea Res. Part II Top. Stud. Oceanogr. **49**: 5365–5375. doi:10.1016/S0967-0645(02)00196-0

Dickson, A. G. 1981. An exact definition of total alkalinity and a procedure for the estimation of alkalinity and total inorganic carbon from titration data. Deep-Sea Res. Part A Oceanogr. Res. Pap. **28**: 609–623.

Dickson, A. G., C. L. Sabine, and J. R. Christian. 2007. Guide to best practices for ocean CO_2 measurements. PICES Special Publication 3, 191 pp.

Duarte, C. M., and others. 2013. Is ocean acidification an open-ocean syndrome? Understanding anthropogenic impacts on seawater pH. Estuaries Coast. **36**: 221–236. doi:10.1007/s12237-013-9594-3

Faber, P. A., V. Evrard, R. J. Woodland, I. C. Cartwright, and P. L. M. Cook. 2014. Pore-water exchange driven by tidal pumping causes alkalinity export in two intertidal inlets. Limnol. Oceanogr. **59**: 1749–1763. doi:10.4319/lo.2014.59.5.1749

FGG Elbe. 2018. Data from data portal of FGG Elbe; [accessed 2018 January 31]. Available from www.fgg-elbe.de

Gattuso, J.-P., M. Frankignoulle, and R. Wollast. 1998. Carbon and carbonate metabolism in coastal aquatic ecosystems. Annu. Rev. Ecol. Syst. **29**: 405–434. doi:10.1146/annurev.ecolsys.29.1.405

Grunwald, M., and others. 2010. Nutrient dynamics in a back barrier tidal basin of the southern North Sea: Time-series, model simulations, and budget estimates. J. Sea Res. **64**: 199–212. doi:10.1016/j.seares.2010.02.008

Gustafsson, E., T. Wällstedt, C. Humborg, C.-M. Mörth, and B. G. Gustafsson. 2014. External total alkalinity loads versus internal generation: The influence of nonriverine alkalinity sources in the Baltic Sea. Global Biogeochem. Cycles **28**: 1358–1370. doi:10.1002/2014GB004888

Hernández-Ayon, J. M., A. Zirino, A. C. Dickson, T. Camiro-Vargas, and E. Valenzuela-Espinoza. 2007. Estimating the contribution of organic bases from microalgae to the titration alkalinity in coastal seawaters. Limnol. Oceanogr.: Methods **5**: 225–232.

Hickel, W., P. Mangelsdorf, and J. Berg. 1993. The human impact in the German Bight: Eutrophication during three decades (1962-1991). Helgolander Meeresunters **47**: 243–263. doi:10.1007/BF02367167

Holt, J., and R. Proctor. 2008. The seasonal circulation and volume transport on the northwest European continental shelf: A fine-resolution model study. J. Geophys. Res. **113**: 1–20. doi:10.1029/2006JC004034

Hoppema, J. M. J. 1993. Carbon dioxide and oxygen disequilibrium in a tidal basin (Dutch Wadden Sea). Neth. J. Sea Res. **31**: 221–229. doi:10.1016/0077-7579(93)90023-L

Hu, X., and W.-J. Cai. 2011*a*. An assessment of ocean margin anaerobic processes on oceanic alkalinity budget. Global Biogeochem. Cycles **25**: 1–11. doi:10.1029/2010gb003859

Hu, X., and W.-J. Cai. 2011*b*. The impact of denitrification on the atmospheric CO_2 uptake potential of seawater. Mar. Chem. **127**: 192–198. doi:10.1016/j.marchem.2011.09.008

Huthnance, J. M. 1997. North Sea interaction with the North Atlantic Ocean. German J. Hydrogr. **49**: 153–162.

Kim, H.-C., K. Lee, and W. Choi. 2006. Contribution of phytoplankton and bacterial cells to the measured alkalinity of seawater. Limnol. Oceanogr. **51**: 331–338. doi:10.4319/lo.2006.51.1.0331

Kitidis, V., and others. 2018. Air-sea CO_2 exchange on the North-West European shelf in 2015.

Krumins, V., M. Gehlen, S. Arndt, P. Van Cappellen, and P. Regnier. 2013. Dissolved inorganic carbon and alkalinity fluxes from coastal marine sediments: Model estimates for different shelf environments and sensitivity to global change. Biogeosciences **10**: 371–398. doi:10.5194/bg-10-371-2013

Kuliński, K., B. Schneider, K. Hammer, U. Machulik, and D. Schulz-Bull. 2014. The influence of dissolved organic matter on the acid–base system of the Baltic Sea. J. Mar. Syst. **132**: 106–115. doi:10.1016/j.jmarsys.2014.01.011

Marencic, H. 2009. Wadden Sea quality status report 2009, p. 597. *In* H. Marencic and J. D. Vlas [eds.].

Millero, F. J., T. B. Graham, F. Huang, H. Bustos-Serrano, and D. Pierrot. 2006. Dissociation constants of carbonic acid in seawater as a function of salinity and temperature. Mar. Chem. **100**: 80–94. doi:10.1016/j.marchem.2005.12.001

Olsen, A., N. Metzl, D. C. E. Bakker, and K. O'Brien. 2015. SOCAT quality control cookbook – for SOCAT version 3, 2015_SOCAT_QC_Cookbook_v3; https://www.socat.info/wp-content/uploads/2017/04/2015_SOCAT_QC_Cookbook_v3.pdf. [accessed 2017 August 21].

Onken, R., and R. Riethmüller. 2010. Determination of the freshwater budget of tidal flats from measurements near a tidal inlet. Cont. Shelf Res. **30**: 924–933. doi:10.1016/j.csr.2010.02.004

Otto, L., J. T. E. Zimmerman, G. K. Furnes, M. Mork, R. Saetre, and G. A. Becker. 1990. Review of the physical oceanography of the North Sea. Neth. J. Sea Res. **26**: 161–238. doi:10.1016/0077-7579(90)90091-T

Painter, S. C., and others. 2018. Terrestrial dissolved organic matter distribution in the North Sea. Sci. Total Environ. **630**: 630–647. doi:10.1016/j.scitotenv.2018.02.237

Pätsch, J., and H.-J. Lenhart. 2011. Daily loads of nutrients, total alkalinity, dissolved inorganic carbon and dissolved organic carbon of the European continental rivers for the years 1977–2009. Univ. of Hamburg.

Pegler, K., and S. Kempe. 1988. The carbonate system of the North Sea: Determination of alkalinity and TCO_2 and calculation of pCO_2 and Si_{Cal} (spring 1986), p. 35–87. *In* S. Kempe, V. Dethlefsen, G. Liebezeit, and U. Harms [eds.], Biogeochemistry and distribution of suspended matter in the North Sea and implications to fisheries biology. Univ. of Hamburg.

Petersen, W. 2014. FerryBox systems: State-of-the-art in Europe and future development. J. Mar. Syst. **140**: 4–12. doi:10.1016/j.jmarsys.2014.07.003

Postma, H. 1981. Exchange of materials between the North Sea and the Wadden Sea. Mar. Geol. **40**: 199–213. doi:10.1016/0025-3227(81)90050-5

Rassmann, J., B. Lansard, L. Pozzato, and C. Rabouille. 2016. Carbonate chemistry in sediment porewaters of the Rhône River delta driven by early diagenesis (northwestern Mediterranean). Biogeosciences **13**: 5379–5394. doi:10.5194/bg-13-5379-2016

Regnier, P., and others. 2013. Anthropogenic perturbation of the carbon fluxes from land to ocean. Nat. Geosci. **6**: 597–607. doi:10.1038/ngeo1830

Salt, L. A., H. Thomas, Y. Bozec, A. V. Borges, and H. J. W. de Baar. 2016. The internal consistency of the North Sea carbonate system. J. Mar. Syst. **157**: 52–64. doi:10.1016/j.jmarsys.2015.11.008

Santos, I. R., K. R. Bryan, C. A. Pilditch, and D. R. Tait. 2014. Influence of porewater exchange on nutrient dynamics in two New Zealand estuarine intertidal flats. Mar. Chem. **167**: 57–70. doi:10.1016/j.marchem.2014.04.006

Santos, I. R., and others. 2015. Porewater exchange as a driver of carbon dynamics across a terrestrial-marine transect: Insights from coupled ^{222}Rn and pCO_2 observations in the German Wadden Sea. Mar. Chem. **171**: 10–20. doi:10.1016/j.marchem.2015.02.005

Schneider, A., D. W. R. Wallace, and A. Körtzinger. 2007. Alkalinity of the Mediterranean Sea. Geophys. Res. Lett. **34**: 1–5.

Schrum, C., and others. 2016. Projected change—North Sea, p. 175–217. *In* M. Quante, F. Colijn (Eds.), North Sea region climate change assessment. Regional climate studies. Springer International Publishing.

Schwichtenberg, F. 2013. Drivers of the carbonate system variability in the southern North Sea: River input, anaerobic alkalinity generation in the Wadden Sea and internal processes. Ph.D. thesis. Univ. of Hamburg.

Stumm, W., and J. J. Morgan. 1981. Aquatic chemistry. An introduction emphasizing chemical equilibria in natural waters, 2nd ed. John Wiley and Sons.

Thomas, H., Y. Bozec, K. Elkalay, and H. J. W. de Baar. 2004. Enhanced open ocean storage of CO_2 from shelf sea pumping. Science **304**: 1005–1008. doi:10.1126/science.1095491

Thomas, H., and others. 2005. The carbon budget of the North Sea. Biogeosciences **2**: 87–96. doi:10.5194/bg-2-87-2005

Thomas, H., and others. 2009. Enhanced ocean carbon storage from anaerobic alkalinity generation in coastal sediments. Biogeosciences **6**: 267–274. doi:10.5194/bg-6-267-2009

Tortell, P. D., and others. 2014. Metabolic balance of coastal Antarctic waters revealed by autonomous pCO_2 and ΔO_2/Ar measurements. Geophys. Res. Lett. **41**: 6803–6810. doi:10.1002/2014GL061266

van Beusekom, J. E. E., U. H. Brockmann, K.-J. Hesse, W. Hickel, K. Poremba, and U. Tillmann. 1999. The importance of sediments in the transformation and turnover of nutrients and organic matter in the Wadden Sea and German Bight. German J. Hydrogr. **51**: 245–266.

van Heuven, S., D. Pierrot, J. W. B. Rae, and D. W. R. Wallace. 2011. MATLAB program developed for CO_2 system calculations. ORNL/CDIAC-105b. Carbon Dioxide Information Analysis Center, Oak Ridge National Laboratory, U.S. Department of Energy.

Voynova, Y. G., K. C. Lebaron, R. T. Barnes, and W. J. Ullman. 2015. In situ response of bay productivity to nutrient loading from a small tributary: The Delaware Bay-Murderkill Estuary tidally-coupled biogeochemical reactor. Estuar. Coast. Shelf Sci. **160**: 33–48. doi:10.1016/j.ecss.2015.03.027

Voynova, Y. G., H. Brix, W. Petersen, W.-K. Sieglinde, and M. Scharfe. 2017. Extreme flood impact on estuarine and coastal biogeochemistry: The 2013 Elbe flood. Biogeosciences **14**: 541–557. doi:10.5194/bg-14-541-2017

Wakelin, S. L., J. T. Holt, J. C. Blackford, J. I. Allen, M. Butenschön, and Y. Artioli. 2012. Modeling the carbon fluxes of the northwest European continental shelf: Validation and budgets. J. Geophys. Res. Oceans **117**: 1–17. doi:10.1029/2011JC007402

Wallmann, K., and others. 2008. Silicate weathering in anoxic marine sediments. Mineral. Mag. **72**: 363–366. doi:10.1180/minmag.2008.072.1.363

Wolf-Gladrow, D. A., R. E. Zeebe, C. Klaas, A. Körtzinger, and A. G. Dickson. 2007. Total alkalinity: The explicit conservative expression and its application to biogeochemical processes. Mar. Chem. **106**: 287–300. doi:10.1016/j.marchem.2007.01.006

Acknowledgments

We thank DFDS Seaways (Copenhagen, Denmark) for the possibility of operating a FerryBox aboard the cargo vessel Hafnia Seaways and gratefully acknowledge the support by the ship's crew. We thank Oliver Wurl and Jochen Wollschläger (University of Oldenburg) and Klas O. Möller (HZG), as well as the crew and participants on the Heincke 491 cruise for collecting discrete DIC/TA samples. Tanja Pieplow and Alina Zacharzewski at HZG helped with the DIC sample analysis. Marit Norli and Kai Sörensen at the Norwegian Institute for Water Research (NIVA) are graciously thanked for measuring and processing TA from discrete samples. We thank three anonymous reviewers for their helpful constructive comments, which substantially improved the structure of the manuscript. This research was partly supported by the EU projects NEXOS (Grant agreement 614102), JERICO-NEXT (Grant agreement 654410), and NIVA Ocean Acidification SIS funding.

Conflict of Interest

None declared.

Submitted 03 June 2018
Revised 12 November 2018
Accepted 16 November 2018

Associate editor: M. Dileep Kumar